

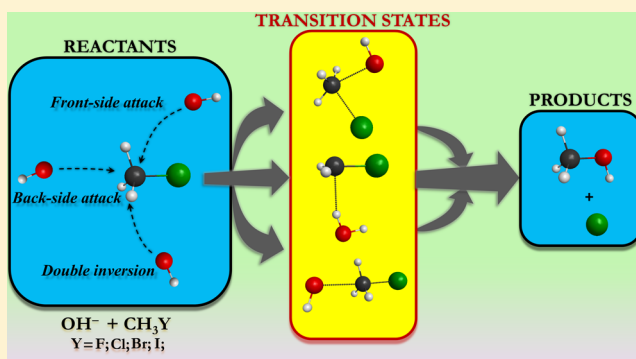
# Benchmark *ab Initio* Characterization of the Inversion and Retention Pathways of the $\text{OH}^- + \text{CH}_3\text{Y}$ [ $\text{Y} = \text{F}, \text{Cl}, \text{Br}, \text{I}$ ] $\text{S}_{\text{N}}2$ Reactions

Domonkos A. Tasi, Zita Fábíán, and Gábor Czakó\*<sup>†</sup>

Department of Physical Chemistry and Materials Science, Institute of Chemistry, University of Szeged, Rerrich Béla tér 1, Szeged H-6720, Hungary

## Supporting Information

**ABSTRACT:** We study the Walden-inversion, front-side attack retention, and double-inversion retention pathways of the  $\text{OH}^- + \text{CH}_3\text{Y}$  [ $\text{Y} = \text{F}, \text{Cl}, \text{Br}, \text{I}$ ]  $\text{S}_{\text{N}}2$  reactions using high-level *ab initio* methods. Benchmark stationary-point structures and frequencies are computed at the CCSD(T)-F12b/aug-cc-pVTZ level of theory and the best technically feasible relative energies are determined on the basis of CCSD(T)-F12b/aug-cc-pVQZ computations complemented with post-CCSD(T) correlation effects at the CCSDT(Q)/aug-cc-pVDZ level, core correlation corrections at the CCSD(T)/aug-cc-pwCVTZ level, scalar relativistic effects using effective core potentials for Br and I, and zero-point energy corrections at the CCSD(T)-F12b/aug-cc-pVTZ level. Walden inversion proceeds via hydrogen-bonded  $\text{HO}^- \cdots \text{HCH}_2\text{Y}$  (Cl, Br, I) complex  $\rightarrow$  hydrogen-bonded  $\text{HO}^- \cdots \text{HCH}_2\text{Y}$  (Cl, Br, I) transition state  $\rightarrow$  ion-dipole  $\text{HO}^- \cdots \text{H}_3\text{CY}$  (F, Cl, Br) complex  $\rightarrow$  Walden-inversion  $[\text{HO}-\text{CH}_3-\text{Y}]^-$  (F, Cl, Br) transition state  $\rightarrow$  hydrogen-bonded  $\text{CH}_3\text{OH} \cdots \text{Y}^-$  (F, Cl, Br, I) complex, where the Y-dependent existence of the submerged stationary points is indicated in parentheses. Front-side  $\text{HO}^- \cdots \text{YCH}_3$  (Cl, Br, I) complexes are also found and  $\text{HO}^- \cdots \text{ICH}_3$  is a deeper minimum than  $\text{HO}^- \cdots \text{HCH}_2\text{I}$ . Front-side attacks go over high barriers of 42.8 (F), 28.7 (Cl), 22.4 (Br), and 17.2 (I) kcal/mol, well above the double-inversion barrier heights of 16.7 (F), 3.4 (Cl), 1.1 (Br), and  $-3.7$  (I) kcal/mol.



## 1. INTRODUCTION

Bimolecular nucleophilic substitution ( $\text{S}_{\text{N}}2$ ) is a widely known reaction class, playing central roles in chemical processes in textbooks, laboratories, and biological environments. The simplest examples of  $\text{S}_{\text{N}}2$  reactions at carbon centers involve the six-atom  $\text{X}^- + \text{CH}_3\text{Y}$  systems, where X and Y are halogens. The traditional textbook mechanism of the  $\text{X}^- + \text{CH}_3\text{Y}$   $\text{S}_{\text{N}}2$  reactions goes through a prereaction  $\text{C}_{3v}$  ion-dipole complex,  $\text{X}^- \cdots \text{H}_3\text{CY}$ , followed by a  $\text{C}_{3v}$  ( $\text{X} \neq \text{Y}$ ) or  $\text{D}_{3h}$  ( $\text{X} = \text{Y}$ ) Walden-inversion transition state (TS),  $[\text{X}-\text{CH}_3-\text{Y}]^-$ , and a post-reaction  $\text{C}_{3v}$  ion-dipole complex,  $\text{XCH}_3 \cdots \text{Y}^-$ .<sup>1</sup> However, recent studies revealed that, especially for  $\text{X} = \text{F}$ , the prereaction complex can be a hydrogen-bonded  $\text{X}^- \cdots \text{HCH}_2\text{Y}$  minimum of  $\text{C}_s$  point-group symmetry and the traditional ion-dipole complex may or may not exist depending on the leaving group and the level of electronic structure theory.<sup>2–5</sup> For the  $\text{F}^- + \text{CH}_3\text{I}$  reaction the existence of the Walden-inversion TS is also questionable, and presumably a hydrogen-bonded  $\text{C}_s$  TS connects the  $\text{F}^- \cdots \text{HCH}_2\text{I}$  and  $\text{FCH}_3 \cdots \text{I}^-$  minima.<sup>2,5</sup> Furthermore, besides the back-side prereaction complexes, front-side complexes of  $\text{X}^- \cdots \text{YCH}_3$   $\text{C}_{3v}$  structures were reported recently<sup>6–8</sup> and were found to play important role in the dynamics of the  $\text{F}^- + \text{CH}_3\text{I}$   $\text{S}_{\text{N}}2$  reaction.<sup>8</sup> That is still not the end of the  $\text{S}_{\text{N}}2$  story, because in 2015 our reaction dynamics simulations revealed a novel double-inversion mechanism for

the  $\text{F}^- + \text{CH}_3\text{Cl}$  reaction.<sup>9</sup> Trajectory animations showed that the double-inversion pathway proceeds via a  $\text{FH} \cdots \text{CH}_2\text{Cl}^-$  TS, which stationary point was later found for all the  $\text{X}^- + \text{CH}_3\text{Y}$  [ $\text{X}, \text{Y} = \text{F}, \text{Cl}, \text{Br}, \text{I}$ ] systems.<sup>10</sup> *Ab initio* computations show that double inversion has a lower barrier than the front-side attack retention pathway in the case of  $\text{F}^-$  nucleophile.<sup>10</sup> In 2017 Hase and co-workers pointed out that double-inversion may not be an intrinsic reaction coordinate (IRC) pathway via the above-mentioned TS.<sup>11</sup> Nevertheless, initiating trajectories from the so-called double-inversion TS results predominantly in substitution with retention of configuration.<sup>11</sup>

Motivated by the above-described recent findings on nontraditional pathways of several six-atom  $\text{S}_{\text{N}}2$  reactions, we aim to extend our investigations toward more complex systems. One way to extend the complexity is to replace methyl halides with ethyl halides as we did recently in our benchmark *ab initio* study on  $\text{F}^- + \text{CH}_3\text{CH}_2\text{Cl}$ , where the double-inversion TS was also found.<sup>12</sup> In the present work we replace the halide nucleophile with  $\text{OH}^-$  and characterize the inversion and retention pathways of the  $\text{OH}^- + \text{CH}_3\text{Y}$  [ $\text{Y} = \text{F}, \text{Cl}, \text{Br}, \text{I}$ ]  $\text{S}_{\text{N}}2$  reactions. These  $\text{OH}^- + \text{CH}_3\text{Y}$  systems have

Received: May 3, 2018

Revised: June 6, 2018

Published: June 7, 2018



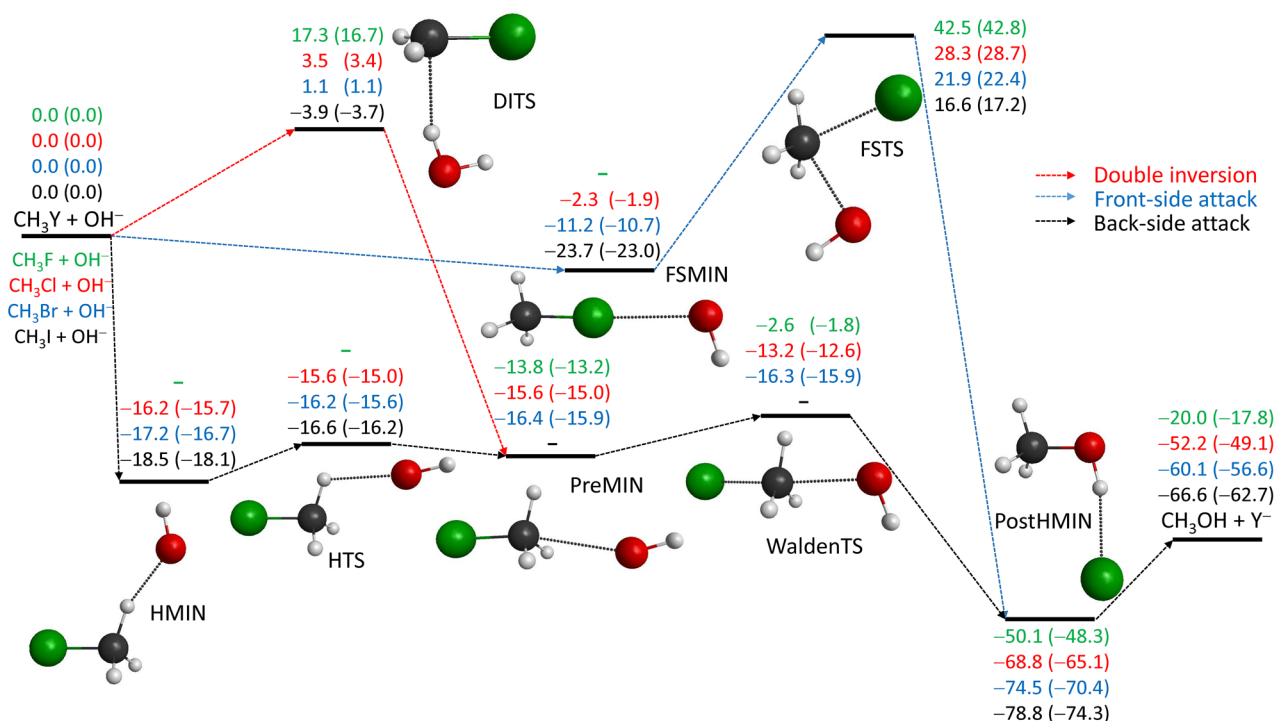


**Figure 1.** Different reaction mechanisms of the  $\text{OH}^- + \text{CH}_3\text{Y}$  [ $\text{Y} = \text{F}, \text{Cl}, \text{Br}, \text{I}$ ]  $\text{S}_{\text{N}}2$  reactions showing the benchmark classical (adiabatic) relative energies, in kcal/mol, of the stationary points obtained as  $\text{QZ} + \delta\text{T} + \delta(\text{Q}) + \Delta\text{core}$  ( $\text{QZ} + \delta\text{T} + \delta(\text{Q}) + \Delta\text{core} + \Delta\text{ZPE}$ ). See Table 1. Note that double inversion may not be an intrinsic reaction coordinate pathway.

been attracted considerable attention in the 21st century sometimes providing surprising results.<sup>13–25</sup> Let us begin with the work of Gonzales et al. that reported in 2001 a hydrogen-bonded postreaction complex,  $\text{CH}_3\text{OH}\cdots\text{F}^-$ , for the  $\text{OH}^- + \text{CH}_3\text{F}$  reaction, whereas the traditional  $\text{HOCH}_3\cdots\text{F}^-$  ion-dipole complex was not found.<sup>13</sup> In 2002 reaction dynamics simulations of Hase and co-workers revealed that the  $\text{OH}^- + \text{CH}_3\text{F}$  reaction avoids the deep minimum corresponding to the hydrogen-bonded  $\text{CH}_3\text{OH}\cdots\text{F}^-$  complex and most of the trajectories proceed directly via the  $\text{HOCH}_3\cdots\text{F}^-$  region, highlighting the fact that dynamics may not follow the minimum-energy pathways.<sup>14</sup> In 2003 two independent studies supported that postreaction ion–dipole complex does not exist for the  $\text{OH}^- + \text{CH}_3\text{F}$   $\text{S}_{\text{N}}2$  reaction,<sup>15,16</sup> and Gonzales et al.<sup>16</sup> reported accurate ab initio data based on MP2/aug-cc-pV5Z and CCSD(T)/aug-cc-pVTZ energy computations considering core and scalar relativistic corrections for three stationary points along the  $\text{S}_{\text{N}}2$  inversion pathway of the  $\text{OH}^- + \text{CH}_3\text{F}$  reaction. For the  $\text{OH}^- + \text{CH}_3\text{Cl}$  reaction Tachikawa and co-workers characterized the prereaction ion–dipole complex, the Walden-inversion TS, and the postreaction complex with MP2/6-311++G(2df,2pd) computations and performed direct dynamics simulations using the HF/3-21+G(d) level of theory.<sup>17,18</sup> The  $\text{OH}^- + \text{CH}_3\text{I}$  reaction has been under very recent experimental and theoretical investigations.<sup>19–22</sup> In 2012 Wester and co-workers<sup>19</sup> studied the effects of water molecules on the dynamics of the  $\text{OH}^- + \text{CH}_3\text{I}$  reaction using the crossed-beam experimental technique. In 2013 Xie et al.<sup>20,21</sup> characterized the stationary points of the  $\text{OH}^- + \text{CH}_3\text{I}$  reaction reporting prereaction and postreaction minima connected by a first-order saddle point, all having hydrogen-bonded structures. Furthermore, a front-side complex,  $\text{HO}^-\cdots\text{ICH}_3$ , was also found at the B97-1/ECP/d level of theory.<sup>20,21</sup> The dynamics and kinetics of the  $\text{OH}^- + \text{CH}_3\text{I}$  reaction were

investigated as well using direct dynamics simulations and the computed results were compared with crossed-beam<sup>20</sup> and selected ion flow tube<sup>21</sup> experiments. In 2015 Hase and co-workers<sup>22</sup> characterized the hydrogen-bonded prereaction complex for  $\text{OH}^- + \text{CH}_3\text{I}$  using B97-1 and MP2 theories with double- and triple- $\zeta$ -quality basis sets. Finally, we note that the mechanisms of the  $\text{OH}^- + \text{CH}_3\text{Y}$  [ $\text{Y} = \text{F}, \text{Cl}, \text{Br}$ ] reactions were also studied in aqueous solution by Wang and co-workers<sup>23–25</sup> using a quantum mechanical molecular mechanics method.

The goal of the present study is to provide a benchmark ab initio characterization of the  $\text{OH}^- + \text{CH}_3\text{Y}$  [ $\text{Y} = \text{F}, \text{Cl}, \text{Br}, \text{I}$ ]  $\text{S}_{\text{N}}2$  reactions moving beyond the previous work in several aspects: (a) We provide a comprehensive study of the above four reactions at the same level of theory, (b) investigate the front-side attack and double-inversion TSs for the first time to the best of our knowledge, (c) use the explicitly correlated CCSD(T)-F12b method ensuring fast basis set convergence for geometry, frequency, and energy computations, and (d) consider core–valence and post-CCSD(T) correlation effects, which were usually neglected in previous studies. The computational details are described in detail in section II. In section III the results are presented and discussed in both qualitative and quantitative points of view. The paper ends with summary and conclusions in section IV.

## II. COMPUTATIONAL DETAILS

The stationary points of the potential energy surfaces of the  $\text{OH}^- + \text{CH}_3\text{Y}$  [ $\text{Y} = \text{F}, \text{Cl}, \text{Br}, \text{I}$ ]  $\text{S}_{\text{N}}2$  reactions are searched and preoptimized at the MP2/aug-cc-pVDZ level of theory, where MP2 denotes second-order Møller–Plesset perturbation theory.<sup>26</sup> Then geometry and harmonic vibrational frequency computations are performed using the explicitly correlated

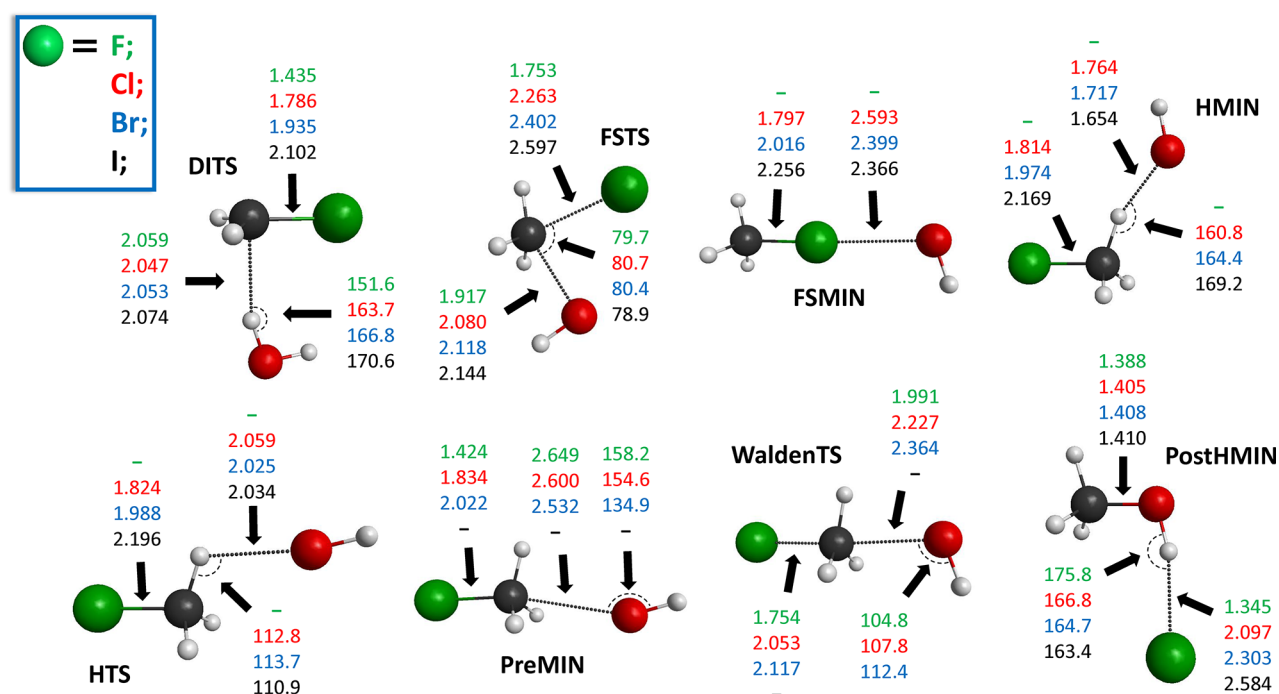


**Figure 2.** Benchmark stationary-point structures for the  $\text{OH}^- + \text{CH}_3\text{Y}$  [ $\text{Y} = \text{F}, \text{Cl}, \text{Br}, \text{I}$ ]  $\text{S}_{\text{N}}2$  reactions showing the most important distances (Å) and angles (deg) obtained at the CCSD(T)-F12b/aug-cc-pVTZ level of theory. All the geometries have  $\text{C}_s$  point-group symmetry, except the nonsymmetric FSTS ( $\text{Y} = \text{F}$ ) and HTS ( $\text{Y} = \text{Br}, \text{I}$ ); see Figure 3.

coupled cluster singles, doubles, and perturbative triples CCSD(T)-F12b method<sup>27</sup> with the correlation-consistent aug-cc-pVDZ and aug-cc-pVTZ basis sets.<sup>28</sup> To obtain the best technically feasible relative energies, the following single-point energy computations are performed at the most accurate CCSD(T)-F12b/aug-cc-pVTZ geometries: (a) CCSD(T)-F12b/aug-cc-pVQZ, (b) CCSD(T),<sup>29</sup> CCSDT,<sup>30</sup> and CCSDT(Q)<sup>31</sup> with the aug-cc-pVDZ basis set, and (c) CCSD(T)/aug-cc-pwCVTZ with both frozen-core and all-electron approaches. For Br and I small-core relativistic effective core potentials,<sup>32</sup> replacing the inner-core  $1s^2 2s^2 2p^6$  and  $1s^2 2s^2 2p^6 3s^2 3p^6 3d^{10}$  electrons, respectively, are used with the corresponding aug-cc-pVDZ-PP, aug-cc-pVTZ-PP, aug-cc-pVQZ-PP, and aug-cc-pwCVTZ-PP basis sets.<sup>32</sup> The frozen-core (FC) computations, used as default unless otherwise noted, correlate the valence electrons only, whereas in the all-electron (AE) approach the  $1s^2$  (C, O, F),  $2s^2 2p^6$  (Cl),  $3s^2 3p^6 3d^{10}$  (Br), and  $4s^2 4p^6 4d^{10}$  (I) electrons are also correlated. All the ab initio computations are performed with the Molpro program package,<sup>33</sup> except CCSDT and CCSDT(Q) that are carried out with the MRCC code<sup>34</sup> interfaced to Molpro.

The benchmark classical relative energies of the stationary points are obtained at the CCSD(T)-F12b/aug-cc-pVTZ geometries as

$$\begin{aligned} &\Delta E(\text{CCSD(T)-F12b/aug-cc-pVQZ}) + \delta[\text{CCSDT}] \\ &+ \delta[\text{CCSDT(Q)}] + \Delta_{\text{core}} \end{aligned} \quad (1)$$

where

$$\begin{aligned} \delta[\text{CCSDT}] &= \Delta E(\text{CCSDT/aug-cc-pVDZ}) \\ &- \Delta E(\text{CCSD(T)/aug-cc-pVDZ}) \end{aligned} \quad (2)$$

$$\begin{aligned} \delta[\text{CCSDT(Q)}] &= \Delta E(\text{CCSDT(Q)/aug-cc-pVDZ}) \\ &- \Delta E(\text{CCSDT/aug-cc-pVDZ}) \end{aligned} \quad (3)$$

and

$$\begin{aligned} \Delta_{\text{core}} &= \Delta E(\text{AE-CCSD(T)/aug-cc-pwCVTZ}) \\ &- \Delta E(\text{FC-CCSD(T)/aug-cc-pwCVTZ}) \end{aligned} \quad (4)$$

The benchmark adiabatic relative energies are computed as

$$\begin{aligned} &\Delta E(\text{CCSD(T)-F12b/aug-cc-pVQZ}) + \delta[\text{CCSDT}] \\ &+ \delta[\text{CCSDT(Q)}] + \Delta_{\text{core}} + \Delta_{\text{ZPE}} \end{aligned} \quad (5)$$

where  $\Delta_{\text{ZPE}}$  is the harmonic zero-point energy correction obtained at the CCSD(T)-F12b/aug-cc-pVTZ level of theory.

### III. RESULTS AND DISCUSSION

A schematic potential energy surface (PES) of the  $\text{OH}^- + \text{CH}_3\text{Y}$  [ $\text{Y} = \text{F}, \text{Cl}, \text{Br}, \text{I}$ ]  $\text{S}_{\text{N}}2$  reactions featuring the benchmark classical and adiabatic energies of the stationary points along the different reaction pathways is shown in Figure 1, and the best structural parameters are given in Figure 2. The relative energies obtained with different ab initio levels of theory such as CCSD(T)-F12b with aug-cc-pVDZ, aug-cc-pVTZ, and aug-cc-pVQZ as well as the post-CCSD(T), core correlation, and ZPE corrections are summarized in Table 1. Furthermore, the interested reader can find all the structural parameters and vibrational frequencies at the MP2/aug-cc-pVDZ, CCSD(T)-F12b/aug-cc-pVDZ, and CCSD(T)-F12b/aug-cc-pVTZ levels of theory in the Supporting Information.

All four  $\text{OH}^- + \text{CH}_3\text{Y}$   $\text{S}_{\text{N}}2$  reactions are exothermic, and the 0 K reaction enthalpies are  $-17.8$ ,  $-49.1$ ,  $-56.6$ , and  $-62.7$  kcal/mol for  $\text{Y} = \text{F}, \text{Cl}, \text{Br}$ , and  $\text{I}$ , respectively. There are several minima and TSs along the back-side attack Walden-inversion

**Table 1. Benchmark Classical and Adiabatic Energies (kcal/mol) of the Stationary Points (Figure 1) Relative to the Reactants for the OH<sup>-</sup> + CH<sub>3</sub>Y [Y = F, Cl, Br, I] S<sub>N</sub>2 Reactions**

OH <sup>-</sup> + CH <sub>3</sub> F	DZ <sup>a</sup>	TZ <sup>b</sup>	QZ <sup>c</sup>	δT <sup>d</sup>	δ(Q) <sup>e</sup>	Δcore <sup>f</sup>	classical <sup>g</sup>	ΔZPE <sup>h</sup>	adiabatic <sup>i</sup>
PreMIN	-13.87	-13.87	-13.74	-0.03	+0.00	+0.01	-13.76	+0.60	-13.16
WaldenTS	-2.44	-2.71	-2.59	-0.10	-0.18	+0.27	-2.60	+0.81	-1.79
PostHMIN	-50.32	-50.19	-50.05	+0.08	+0.08	-0.16	-50.05	+1.75	-48.31
FSTS	42.56	42.44	42.74	-0.13	-0.43	+0.32	42.49	+0.36	42.85
DITS	17.00	17.23	17.45	-0.04	-0.02	-0.10	17.29	-0.55	16.73
F <sup>-</sup> + CH <sub>3</sub> OH	-19.76	-19.82	-19.95	+0.01	+0.11	-0.15	-19.97	+2.19	-17.78
OH <sup>-</sup> + CH <sub>3</sub> Cl	DZ <sup>a</sup>	TZ <sup>b</sup>	QZ <sup>c</sup>	δT <sup>d</sup>	δ(Q) <sup>e</sup>	Δcore <sup>f</sup>	classical <sup>g</sup>	ΔZPE <sup>h</sup>	adiabatic <sup>i</sup>
HMIN	-16.39	-16.33	-16.20	-0.02	+0.01	+0.01	-16.20	+0.55	-15.66
HTS	-15.47	-15.64	-15.55	-0.03	-0.01	+0.03	-15.56	+0.52	-15.04
PreMIN	-15.49	-15.71	-15.62	-0.04	-0.01	+0.05	-15.61	+0.58	-15.03
WaldenTS	-12.83	-13.26	-13.21	-0.11	-0.17	+0.28	-13.21	+0.62	-12.59
PostHMIN	-68.77	-68.91	-69.04	+0.07	+0.21	-0.01	-68.77	+3.63	-65.13
FSMIN	-2.74	-2.38	-2.24	-0.03	-0.09	+0.01	-2.35	+0.43	-1.92
FSTS	28.92	28.64	28.81	-0.19	-0.66	+0.35	28.31	+0.39	28.70
DITS	3.31	3.51	3.60	+0.04	+0.00	-0.10	3.54	-0.13	3.42
Cl <sup>-</sup> + CH <sub>3</sub> OH	-52.10	-52.37	-52.65	+0.06	+0.26	+0.08	-52.25	+3.17	-49.08
OH <sup>-</sup> + CH <sub>3</sub> Br	DZ <sup>a</sup>	TZ <sup>b</sup>	QZ <sup>c</sup>	δT <sup>d</sup>	δ(Q) <sup>e</sup>	Δcore <sup>f</sup>	classical <sup>g</sup>	ΔZPE <sup>h</sup>	adiabatic <sup>i</sup>
HMIN	-17.54	-17.33	-17.17	-0.02	+0.01	+0.04	-17.15	+0.48	-16.68
HTS	-16.30	-16.28	-16.17	-0.04	-0.01	+0.04	-16.18	+0.57	-15.60
PreMIN	-16.53	-16.53	-16.41	-0.05	-0.04	+0.08	-16.43	+0.50	-15.93
WaldenTS	-16.24	-16.33	-16.24	-0.09	-0.14	+0.19	-16.28	+0.34	-15.94
PostHMIN	-74.98	-74.75	-74.95	+0.07	+0.24	+0.10	-74.54	+4.12	-70.42
FSMIN	-11.37	-11.33	-11.21	+0.02	-0.23	+0.18	-11.24	+0.54	-10.70
FSTS	22.51	22.30	22.44	-0.16	-0.71	+0.37	21.93	+0.44	22.36
DITS	0.63	0.89	1.01	+0.05	-0.01	+0.06	1.11	+0.01	1.11
Br <sup>-</sup> + CH <sub>3</sub> OH	-60.59	-60.41	-60.80	+0.07	+0.29	+0.32	-60.13	+3.58	-56.55
OH <sup>-</sup> + CH <sub>3</sub> I	DZ <sup>a</sup>	TZ <sup>b</sup>	QZ <sup>c</sup>	δT <sup>d</sup>	δ(Q) <sup>e</sup>	Δcore <sup>f</sup>	classical <sup>g</sup>	ΔZPE <sup>h</sup>	adiabatic <sup>i</sup>
HMIN	-18.89	-18.64	-18.48	-0.02	+0.00	+0.02	-18.49	+0.42	-18.07
HTS	-16.74	-16.69	-16.57	-0.04	-0.04	+0.01	-16.65	+0.50	-16.15
PostHMIN	-79.30	-79.08	-79.43	+0.09	+0.27	+0.29	-78.78	+4.49	-74.29
FSMIN	-24.09	-24.10	-24.05	+0.07	-0.23	+0.51	-23.69	+0.68	-23.01
FSTS	17.19	17.03	17.10	-0.11	-0.79	+0.42	16.62	+0.58	17.20
DITS	-4.20	-4.13	-4.05	+0.07	-0.01	+0.15	-3.85	+0.18	-3.67
I <sup>-</sup> + CH <sub>3</sub> OH	-67.16	-67.08	-67.71	+0.08	+0.31	+0.67	-66.64	+3.98	-62.67

<sup>a</sup>CCSD(T)-F12b/aug-cc-pVDZ. <sup>b</sup>CCSD(T)-F12b/aug-cc-pVTZ. <sup>c</sup>CCSD(T)-F12b/aug-cc-pVQZ. <sup>d</sup>CCSDT/aug-cc-pVDZ - CCSD(T)/aug-cc-pVDZ. <sup>e</sup>CCSDT(Q)/aug-cc-pVDZ - CCSDT/aug-cc-pVDZ. <sup>f</sup>AE-CCSD(T)/aug-cc-pwCVTZ - FC-CCSD(T)/aug-cc-pwCVTZ. <sup>g</sup>QZ + δT + δ(Q) + Δcore. <sup>h</sup>ΔZPE(CCSD(T)-F12b/aug-cc-pVTZ). <sup>i</sup>QZ + δT + δ(Q) + Δcore + ΔZPE.

reaction pathway, and all of them are below the reactant asymptote. The global minimum of the PESs corresponds to exit-channel complexes, which are not the usual ion-dipole complexes with Y<sup>-</sup>⋯CH<sub>3</sub>OH structures, but hydrogen-bonded CH<sub>3</sub>OH⋯Y<sup>-</sup> complexes (PostHMIN) as seen in Figure 1. For Y = F, a hydrogen-bonded F<sup>-</sup>⋯HCH<sub>3</sub>OH complex (Table S4) is also found with an energy ~21 kcal/mol higher than that of CH<sub>3</sub>OH⋯F<sup>-</sup>. As mentioned earlier, trajectory simulations showed that the OH<sup>-</sup> + CH<sub>3</sub>F reaction avoids this PostHMIN configuration and proceeds via the usual backward scattering mechanism.<sup>14</sup> The F<sup>-</sup> leaving group forms the strongest OH⋯Y<sup>-</sup> hydrogen bond with a dissociation energy (*D*<sub>0</sub>) of 30.5 kcal/mol, whereas the *D*<sub>0</sub> values are 16.0, 13.8, and 11.6 kcal/mol for Y = Cl, Br, and I, respectively. These dissociation energies are in accord with the trends of the H⋯Y<sup>-</sup> distances of 1.345, 2.097, 2.303, and 2.584 Å for Y = F, Cl, Br, and I, respectively (Figure 2). The entrance channels of the title reactions are also nontraditional, except for Y = F. The OH<sup>-</sup> + CH<sub>3</sub>F reaction proceeds via an ion-dipole complex (PreMIN) followed by a usual Walden-inversion TS (WaldenTS), as seen in Figure 1. Here the barrier is just slightly submerged by 2.6

(1.8) kcal/mol without (with) ZPE correction. In the cases of Cl and Br leaving groups, a hydrogen-bonded prereaction complex (HMIN) also exists besides PreMIN and a first-order saddle point (HTS) connects the two minima. HMIN is below PreMIN by 0.6–0.8 kcal/mol, and the barrier between them is negligible. For Y = Cl the classical (adiabatic) energy of the WaldenTS is -13.2 (-12.6) kcal/mol relative to the reactants, which is 2.4 kcal/mol above PreMIN. For Y = Br the energies of PreMIN and WaldenTS, -16.4 (-15.9) and -16.3 (-15.9) kcal/mol, are the same within 0.1 kcal/mol. Moreover, for Y = I the traditional PreMIN and WaldenTS do not exist anymore and the reaction proceeds via HMIN → HTS → PostHMIN. Here HMIN is at -18.5 (-18.1) kcal/mol, below HTS by 1.9 kcal/mol. This finding is in qualitative agreement with the DFT/B97-1/ECP/d results of Xie et al.,<sup>20,21</sup> though our benchmark energies are above the DFT values by 1.5–2 kcal/mol. As Figure 2 shows, the H⋯OH hydrogen bond is decreasing as 1.764, 1.717, and 1.654 Å for Y = Cl, Br, and I in accord with the leaving-group dependence of the depth of HMIN. The corresponding HTS values of 2.059, 2.025, and 2.034 Å are longer and do not show significant Y dependence.

However, we have found a qualitative difference between the HTSs of the  $Y = \text{Cl}$  and  $Y = \text{Br, I}$  systems, because the former has  $C_s$ , whereas the latter structures have  $C_1$  symmetries, as shown in Figure 3.

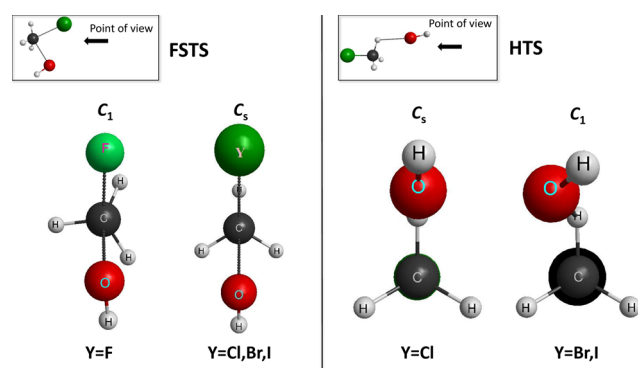


**Figure 3.** Point-group symmetries of the FSTS and HTS structures with different halogens.

For the  $\text{OH}^- + \text{CH}_3\text{Y}$  [ $Y = \text{Cl, Br, I}$ ] systems, we find front-side complexes (FSMIN) in the entrance channels, where  $\text{OH}^-$  connects to  $Y$ . As Figure 2 shows, FSMIN complexes have  $C_s$  structures with almost collinear  $\text{C}-\text{Y}\cdots\text{O}$  arrangements and  $\text{Y}\cdots\text{O}$  distances of 2.593, 2.399, and 2.366 Å for  $Y = \text{Cl, Br, and I}$ , respectively. For  $Y = \text{Cl}$  FSMIN is just slightly bonded with dissociation energy around 2 kcal/mol, whereas for  $Y = \text{Br}$  and  $\text{I}$  the  $D_0$  values are 10.7 and 23.0 kcal/mol, respectively. Thus, for  $Y = \text{I}$  FSMIN is deeper than HMIN by 4.9 kcal/mol, which may play an important role in the dynamics, similar to the case of the  $\text{F}^- + \text{CH}_3\text{I}$  reaction, where significant front-side complex formation was recently revealed.<sup>8</sup> Note that Hase and co-workers<sup>20,21</sup> also reported this front-side complex for the  $\text{OH}^- + \text{CH}_3\text{I}$  system, but their B97-1/ECP/d method provided a minimum 2.4 kcal/mol deeper than the present benchmark result.

Besides the Walden-inversion pathways, the title reactions can proceed via the front-side attack and double-inversion retention mechanisms, as also shown in Figure 1. Front-side attack goes through a high-energy barrier of 42.8, 28.7, 22.4, and 17.2 kcal/mol for  $Y = \text{F, Cl, Br, and I}$ , respectively, whereas the corresponding double-inversion barrier heights are 16.7, 3.4, 1.1, and  $-3.7$  kcal/mol, in order. Thus, similar to the  $\text{F}^- + \text{CH}_3\text{Y}$  reactions,<sup>35</sup> double inversion opens a lower-energy reaction path, compared to the front-side attack pathway, which can result in retention of configuration in the  $\text{OH}^- + \text{CH}_3\text{Y}$   $\text{S}_\text{N}2$  reactions. Moreover, for the first time, in the case of

the  $\text{OH}^- + \text{CH}_3\text{I}$  reaction we find a submerged double-inversion barrier, in principle, allowing retention at very low collision energies. At the front-side attack transition state (FSTS) the  $\text{C}-\text{Y}$  distances are 1.753, 2.263, 2.402, and 2.597 Å for  $Y = \text{F, Cl, Br, and I}$ , respectively, stretched by 0.369, 0.481, 0.461, and 0.454 Å relative to the corresponding bond length in  $\text{CH}_3\text{Y}$ . The  $\text{C}-\text{O}$  distances are longer by 0.497, 0.660, 0.698, and 0.724 Å than the  $\text{C}-\text{O}$  bond length of 1.420 Å in  $\text{CH}_3\text{OH}$ . The  $\text{Y}-\text{C}-\text{O}$  angles are around  $80^\circ$  for all four systems. For  $Y = \text{Cl, Br, and I}$  FSTS has  $C_s$  symmetry, whereas in the case of  $Y = \text{F}$  the symmetry is slightly broken, as shown in Figure 3. The double-inversion transition state (DITS) has  $C_s$  symmetry, where the  $\text{CH}_2\text{Y}^-$  unit is almost planar and  $\text{H}_2\text{O}$  connects to the  $\text{C}$  atom with a hydrogen bond of around 2.1 Å length in all four cases. The DITSs have substantial imaginary frequencies of 983i (F), 864i (Cl), 889i (Br), and 846i (I)  $\text{cm}^{-1}$  at the CCSD(T)-F12b/aug-cc-pVTZ level of theory, whereas the corresponding FSTS values are 729i, 627i, 578i, and 545i  $\text{cm}^{-1}$ , in order, as seen in the Supporting Information. The large imaginary frequencies of the DITSs may make these TSs stand out from the other proton-transfer-like stationary points of the  $\text{OH}^- + \text{CH}_3\text{Y}$  systems. At this point, we should note that the double-inversion pathway shown in Figure 1 may be a non-IRC pathway as Hase and co-workers<sup>11</sup> pointed out in the case of the  $\text{F}^- + \text{CH}_3\text{I}$  reaction.

The detailed data presented in Table 1 and shown in Figures 4 and 5 allow estimating the accuracy of the new benchmark relative energies. Figure 4 shows the fast basis-set convergence of the explicitly correlated CCSD(T)-F12b method, since both the aug-cc-pVDZ and aug-cc-pVTZ basis sets provide similar quality results with 0.1–0.2 kcal/mol deviations from the aug-cc-pVQZ relative energies for most of the stationary points. The largest deviation of about 0.6 kcal/mol is found for the  $\text{I}^- + \text{CH}_3\text{OH}$  product channel, whereas the mean absolute deviations of the aug-cc-pVDZ and aug-cc-pVTZ data, relative to aug-cc-pVQZ, are only 0.22 and 0.16 kcal/mol, respectively, considering all 31 stationary points shown in Figure 4. As Table 1 and Figure 5 show, the post-CCSD(T) correlation effects are usually small, typically between 0 and  $\pm 0.3$  kcal/mol. The most significant effects are found for FSTS, where the post-CCSD(T) correlation energy contributions are  $-0.56$ ,  $-0.85$ ,  $-0.87$ , and  $-0.90$  kcal/mol for  $Y = \text{F, Cl, Br, and I}$ , respectively. As Figure 5 shows, the signs of the  $\delta[\text{CCSDT}]$  and  $\delta[\text{CCSDT}(\text{Q})]$  energy increments are almost always the same and the latter is usually larger, whereas the core correlation corrections often have opposite signs and magnitudes similar to those of the post-CCSD(T) corrections; thus the post-CCSD(T) and core corrections can partially cancel each other. This is not always the case, especially for the

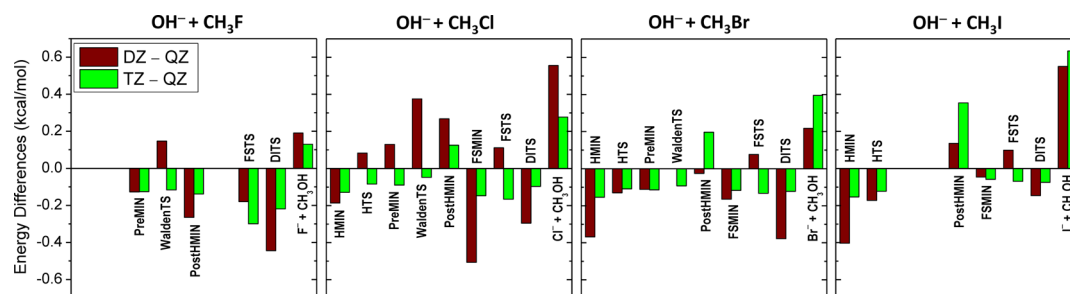


**Figure 4.** Convergence of the CCSD(T)-F12b relative energies with the aug-cc-pVDZ (DZ), aug-cc-pVTZ (TZ), and aug-cc-pVQZ (QZ) basis sets for the different stationary points of the  $\text{OH}^- + \text{CH}_3\text{Y}$  [ $Y = \text{F, Cl, Br, I}$ ]  $\text{S}_\text{N}2$  reactions.

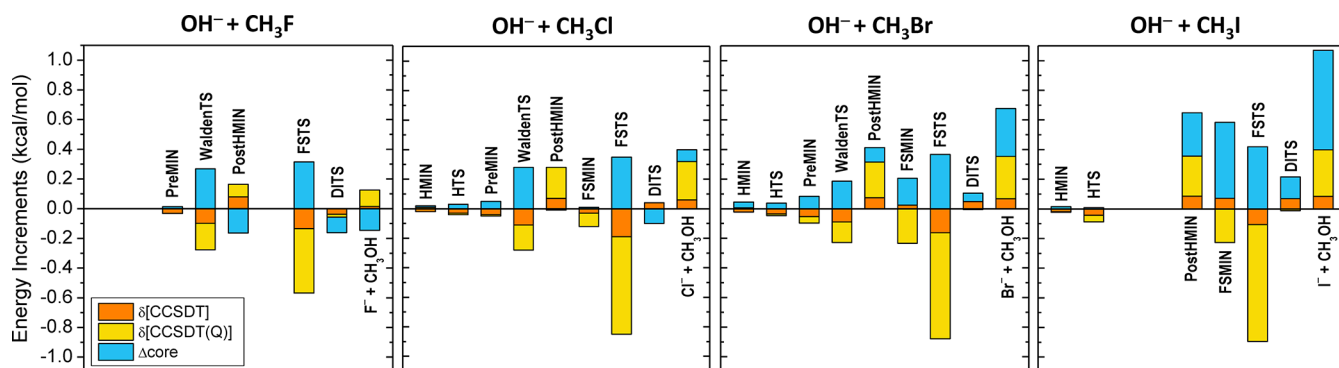


**Figure 5.** Post-CCSD(T), eqs 2 and 3, and core, eq 4, correlation energy effects for the different stationary points of the  $\text{OH}^- + \text{CH}_3\text{Y}$  [ $\text{Y} = \text{F}, \text{Cl}, \text{Br}, \text{I}$ ]  $\text{S}_{\text{N}}2$  reactions.

$\text{Y}^- + \text{CH}_3\text{OH}$  [ $\text{Y} = \text{Cl}, \text{Br}, \text{and I}$ ] product channels, where the post-CCSD(T) and core-correlation effects are both positive and result in cumulative energy corrections of 0.40, 0.68, and 1.07 kcal/mol, respectively. Thus, these results show that these traditionally neglected effects should be taken into account if subchemical accuracy is desired for some of the reaction enthalpies. Relativistic effects are expected to be significant for Br and I, where scalar relativity is involved in the effective core potentials used in the present study. For the other atoms the scalar relativistic corrections are likely to be small, usually 10–50% of the core correlation effects;<sup>36</sup> thus these are neglected in this study. Spin-orbit corrections are also negligible for these closed-shell systems. As Table 1 shows, ZPE effects are around 0.5 kcal/mol for most of the stationary points, except for PostHMINs and the products, where  $\Delta\text{ZPEs}$  are in the range 1.7–4.5 kcal/mol and increase from  $\text{Y} = \text{F}$  to  $\text{I}$ . Thus, ZPE corrections should be considered to obtain chemically accurate reaction enthalpies for the  $\text{OH}^- + \text{CH}_3\text{Y}$  [ $\text{Y} = \text{F}, \text{Cl}, \text{Br}, \text{I}$ ]  $\text{S}_{\text{N}}2$  reactions. On the basis of the above analysis of the energy convergence and contributions, one can conclude that the present benchmark relative energies are usually accurate with a small, about  $\pm 0.3$  kcal/mol uncertainty.

For the reaction enthalpies we can directly check the accuracy of the above predictions by comparing the computed values to “experiment”. On the basis of the 0 K gas-phase enthalpies of formation data taken from the experiment- and theory-based active thermochemical tables (ATcT),<sup>37</sup> we can obtain enthalpies of  $-17.66 \pm 0.07$ ,  $-49.10 \pm 0.07$ ,  $-56.64 \pm 0.08$ , and  $-62.91 \pm 0.06$  kcal/mol for the  $\text{OH}^- + \text{CH}_3\text{Y} \rightarrow \text{Y}^- + \text{CH}_3\text{OH}$  [ $\text{Y} = \text{F}, \text{Cl}, \text{Br}, \text{I}$ ] reactions, respectively,<sup>38</sup> in excellent agreement with the present ab initio results of  $-17.78$ ,  $-49.08$ ,  $-56.55$ , and  $-62.67$  kcal/mol, in order. As seen, all the ATcT and the new ab initio reaction enthalpies agree within  $\pm 0.3$  kcal/mol, or in most cases much better, confirming the above uncertainty predictions and the accuracy of the present benchmark results.

The new definitive benchmark data allow assessing the accuracy of the previous computations. For the  $\text{OH}^- + \text{CH}_3\text{F}$   $\text{S}_{\text{N}}2$  reaction the Walden-inversion channel was characterized by various electronic structure levels of theory.<sup>13,15,16</sup> MP2 has an accuracy of  $\pm 1$  kcal/mol with a triple- $\zeta$  basis, except for PostHMIN, where MP2 gives a too deep minimum by about 2 kcal/mol.<sup>15</sup> CCSD(T)/triple- $\zeta$  usually has chemical accuracy providing agreement with the present benchmark energies within 1 kcal/mol.<sup>13,15</sup> For PreMIN, WaldenTS, PostHMIN, and  $\text{F}^- + \text{CH}_3\text{OH}$  stationary points of the  $\text{OH}^- + \text{CH}_3\text{F}$  reaction accurate focal-point energies of  $-13.02$ ,  $-1.81$ ,

$-48.48$ , and  $-17.87$  kcal/mol, respectively, are also available,<sup>16</sup> which are in very good agreement with the corresponding new benchmark data of  $-13.16$ ,  $-1.79$ ,  $-48.31$ , and  $-17.78$  kcal/mol. Among the other three reactions, perhaps the most notable results are the B97-1 energies corresponding to the Walden-inversion pathway of the  $\text{OH}^- + \text{CH}_3\text{I}$  reaction,<sup>20,21</sup> which usually have an error of about 2 kcal/mol relative to the present benchmark energies. The front-side attack and double-inversion pathways are reported for the first time for the title reactions; therefore, their properties cannot be compared to literature data.

#### IV. SUMMARY AND CONCLUSIONS

We have performed a high-level ab initio study for the  $\text{OH}^- + \text{CH}_3\text{Y}$  [ $\text{Y} = \text{F}, \text{Cl}, \text{Br}, \text{I}$ ]  $\text{S}_{\text{N}}2$  reactions providing qualitatively and quantitatively new results. On the qualitative side, we have characterized the front-side attack and double-inversion retention pathways for the first time in the case of the title reactions, to the best of our knowledge. The computations reveal that double inversion has a smaller barrier than front-side attack. Moreover, for  $\text{Y} = \text{I}$  double inversion is a barrierless process via a submerged transition state. Furthermore, in agreement with, and in some cases, extending previous studies,<sup>13–15,20,21</sup> we find that the Walden-inversion pathways of the  $\text{OH}^- + \text{CH}_3\text{Y}$   $\text{S}_{\text{N}}2$  reactions are nontraditional in several aspects: (1) In the postreaction region hydrogen-bonded  $\text{CH}_3\text{OH}\cdots\text{Y}^-$  complexes exist instead of the traditional ion-dipole complexes. (2) For  $\text{Y} = \text{Cl}$  and  $\text{Br}$  there are hydrogen-bonded  $\text{HO}^-\cdots\text{HCH}_2\text{Y}$  complexes in the entrance channels, whose energies are slightly below the ion-dipole  $\text{HO}^-\cdots\text{H}_3\text{CY}$  minima and hydrogen-bonded transition states connect the  $\text{HO}^-\cdots\text{HCH}_2\text{Y}$  and  $\text{HO}^-\cdots\text{H}_3\text{CY}$  minima. (3) For  $\text{Y} = \text{I}$  the traditional ion-dipole complex and Walden-inversion TS are not found and the  $\text{OH}^- + \text{CH}_3\text{I}$  reaction proceeds via the hydrogen-bonded minimum and transition state. (4) For  $\text{Y} = \text{Cl}, \text{Br}, \text{I}$ ,  $\text{HO}^-\cdots\text{YCH}_3$  front-side complexes are found and in the case of  $\text{Y} = \text{I}$  this front-side complex is the global minimum of the entrance channel. On the quantitative side, we provide new benchmark data based on CCSD(T)-F12b/aug-cc-pVTZ geometries and vibrational frequencies as well as energies obtained at CCSD(T)-F12b/aug-cc-pVQZ with additive core and post-CCSD(T) correlation corrections. We show that most of the new benchmark energies are accurate within about 0.3 kcal/mol, because the explicitly correlated CCSD(T)-F12b method has fast basis set convergence and the core and post-CCSD(T) effects are taken into account. The latter is not always important, because the core and post-CCSD(T)

corrections of about 0.3 kcal/mol often partially cancel each other, except for most of the postreaction complexes and products, where these auxiliary corrections can add up to 1 kcal/mol. ZPE effects are also considered, which are found essential for accurate reaction enthalpies.

In the present study we have focused on the most important reaction channel of the  $\text{OH}^- + \text{CH}_3\text{Y}$  reactions. Besides  $\text{S}_{\text{N}}2$ , proton transfer can also occur and, on the basis of previous studies, many stationary points are involved in the proton-abstraction process.<sup>21</sup> The detailed ab initio study of this higher-energy channel may be considered in a future work. Furthermore, as some previous work revealed,<sup>14,11</sup> the title reactions, and similar systems, may not follow IRC pathways; thus reaction dynamics simulations would be desired to gain deeper insights into the dynamics of the title reactions. As mentioned earlier, Hase and co-workers<sup>14,20,21</sup> reported trajectory studies for  $\text{OH}^- + \text{CH}_3\text{Y}$  reactions using the direct dynamics approach. We plan to use our analytic-PES-based method<sup>35</sup> to study the dynamics of the  $\text{OH}^- + \text{CH}_3\text{I}$  reaction, which may provide double inversion without activation energy. PES development is underway in our group, for which the present benchmark stationary-point properties provide a definitive guidance.

## ■ ASSOCIATED CONTENT

### Supporting Information

The Supporting Information is available free of charge on the ACS Publications website at DOI: 10.1021/acs.jpca.8b04218.

Energies, structures, and frequencies of the stationary points at different levels of theory (PDF)

## ■ AUTHOR INFORMATION

### Corresponding Author

\*G. Czakó. E-mail: gczako@chem.u-szeged.hu.

### ORCID

Gábor Czakó: 0000-0001-5136-4777

### Notes

The authors declare no competing financial interest.

## ■ ACKNOWLEDGMENTS

G.C. thanks the National Research, Development and Innovation Office–NKFIH, K-125317 for financial support. We acknowledge the National Information Infrastructure Development Institute for awarding us access to resource based in Hungary at Szeged.

## ■ REFERENCES

- (1) Ingold, C. K. *Structure and Mechanisms in Organic Chemistry*; Cornell Univ. Press: Ithaca, NY, 1953.
- (2) Zhang, J.; Hase, W. L. Electronic Structure Theory Study of the  $\text{F}^- + \text{CH}_3\text{I} \rightarrow \text{FCH}_3 + \text{I}^-$  Potential Energy Surface. *J. Phys. Chem. A* **2010**, *114*, 9635–9643.
- (3) Zhang, J.; Mikosch, J.; Trippel, S.; Otto, R.; Weidemüller, M.; Wester, R.; Hase, W. L.  $\text{F}^- + \text{CH}_3\text{I} \rightarrow \text{FCH}_3 + \text{I}^-$  Reaction Dynamics. Nontraditional Atomistic Mechanisms and Formation of a Hydrogen-Bonded Complex. *J. Phys. Chem. Lett.* **2010**, *1*, 2747–2752.
- (4) Szabó, I.; Császár, A. G.; Czakó, G. Dynamics of the  $\text{F}^- + \text{CH}_3\text{Cl} \rightarrow \text{Cl}^- + \text{CH}_3\text{F}$   $\text{S}_{\text{N}}2$  Reaction on a Chemically Accurate Potential Energy Surface. *Chem. Sci.* **2013**, *4*, 4362–4370.
- (5) Gyóri, T.; Olasz, B.; Paragi, G.; Czakó, G. Effects of the Level of Electronic Structure Theory on the Dynamics of the  $\text{F}^- + \text{CH}_3\text{I}$  Reaction. *J. Phys. Chem. A* **2018**, *122*, 3353–3364.

- (6) Stei, M.; Carrascosa, E.; Kainz, M. A.; Kelkar, A. H.; Meyer, J.; Szabó, I.; Czakó, G.; Wester, R. Influence of the Leaving Group on the Dynamics of a Gas-Phase  $\text{S}_{\text{N}}2$  Reaction. *Nat. Chem.* **2016**, *8*, 151–156.

- (7) Olasz, B.; Szabó, I.; Czakó, G. High-Level ab Initio Potential Energy Surface and Dynamics of the  $\text{F}^- + \text{CH}_3\text{I}$   $\text{S}_{\text{N}}2$  and Proton-Transfer Reactions. *Chem. Sci.* **2017**, *8*, 3164–3170.

- (8) Szabó, I.; Olasz, B.; Czakó, G. Deciphering Front-Side Complex Formation in  $\text{S}_{\text{N}}2$  Reactions via Dynamics Mapping. *J. Phys. Chem. Lett.* **2017**, *8*, 2917–2923.

- (9) Szabó, I.; Czakó, G. Revealing a Double-Inversion Mechanism for the  $\text{F}^- + \text{CH}_3\text{Cl}$   $\text{S}_{\text{N}}2$  Reaction. *Nat. Commun.* **2015**, *6*, 5972.

- (10) Szabó, I.; Czakó, G. Double-Inversion Mechanisms of the  $\text{X}^- + \text{CH}_3\text{Y}$  [ $\text{X}, \text{Y} = \text{F}, \text{Cl}, \text{Br}, \text{I}$ ]  $\text{S}_{\text{N}}2$  Reactions. *J. Phys. Chem. A* **2015**, *119*, 3134–3140.

- (11) Ma, Y.-T.; Ma, X.; Li, A.; Guo, H.; Yang, L.; Zhang, J.; Hase, W. L. Potential Energy Surface Stationary Points and Dynamics of the  $\text{F}^- + \text{CH}_3\text{I}$  Double Inversion Mechanism. *Phys. Chem. Chem. Phys.* **2017**, *19*, 20127–20136.

- (12) Tajti, V.; Czakó, G. Benchmark ab Initio Characterization of the Complex Potential Energy Surface of the  $\text{F}^- + \text{CH}_3\text{CH}_2\text{Cl}$  Reaction. *J. Phys. Chem. A* **2017**, *121*, 2847–2854.

- (13) Gonzales, J. M.; Cox, R. S.; Brown, S. T.; Allen, W. D.; Schaefer, H. F. Assessment of Density Functional Theory for Model  $\text{S}_{\text{N}}2$  Reactions:  $\text{CH}_3\text{X} + \text{F}^-$  ( $\text{X} = \text{F}, \text{Cl}, \text{CN}, \text{OH}, \text{SH}, \text{NH}_2, \text{PH}_2$ ). *J. Phys. Chem. A* **2001**, *105*, 11327–11346.

- (14) Sun, L.; Song, K.; Hase, W. L. A  $\text{S}_{\text{N}}2$  Reaction That Avoids Its Deep Potential Energy Minimum. *Science* **2002**, *296*, 875–878.

- (15) Sun, L.; Song, K.; Hase, W. L.; Sena, M.; Riveros, J. M. Stationary Points for the  $\text{OH}^- + \text{CH}_3\text{F} \rightarrow \text{CH}_3\text{OH} + \text{F}^-$  Potential Energy Surface. *Int. J. Mass Spectrom.* **2003**, *227*, 315–325.

- (16) Gonzales, J. M.; Pak, C.; Cox, R. S.; Allen, W. D.; Schaefer, H. F., III; Császár, A. G.; Tarczay, G. Definitive ab Initio Studies of Model  $\text{S}_{\text{N}}2$  Reactions  $\text{CH}_3\text{X} + \text{F}^-$  ( $\text{X} = \text{F}, \text{Cl}, \text{CN}, \text{OH}, \text{SH}, \text{NH}_2, \text{PH}_2$ ). *Chem. - Eur. J.* **2003**, *9*, 2173–2192.

- (17) Tachikawa, H.; Igarashi, M.; Ishibashi, T. A Direct ab Initio Trajectory Study on the Gas-Phase  $\text{S}_{\text{N}}2$  Reaction  $\text{OH}^- + \text{CH}_3\text{Cl} \rightarrow \text{CH}_3\text{OH} + \text{Cl}^-$ . *J. Phys. Chem. A* **2002**, *106*, 10977–10984.

- (18) Tachikawa, H.; Igarashi, M. Direct ab Initio Molecular Dynamics Study on a  $\text{S}_{\text{N}}2$  Reaction  $\text{OH}^- + \text{CH}_3\text{Cl} \rightarrow \text{CH}_3\text{OH} + \text{Cl}^-$ : Effect of Non-Zero Impact Parameter on the Reaction Dynamics. *Chem. Phys.* **2006**, *324*, 639–646.

- (19) Otto, R.; Brox, J.; Trippel, S.; Stei, M.; Best, T.; Wester, R. Single Solvent Molecules Can Affect the Dynamics of Substitution Reactions. *Nat. Chem.* **2012**, *4*, 534–538.

- (20) Xie, J.; Sun, R.; Siebert, M. R.; Otto, R.; Wester, R.; Hase, W. L. Direct Dynamics Simulations of the Product Channels and Atomistic Mechanisms for the  $\text{OH}^- + \text{CH}_3\text{I}$  Reaction. Comparison with Experiment. *J. Phys. Chem. A* **2013**, *117*, 7162–7178.

- (21) Xie, J.; Kohale, S. C.; Hase, W. L.; Ard, S. G.; Melko, J. J.; Shuman, N. S.; Viggiano, A. A. Temperature Dependence of the  $\text{OH}^- + \text{CH}_3\text{I}$  Reaction Kinetics. Experimental and Simulation Studies and Atomic-Level Dynamics. *J. Phys. Chem. A* **2013**, *117*, 14019–14027.

- (22) Xie, J.; Zhang, J.; Hase, W. L. Is There Hydrogen Bonding for Gas Phase  $\text{S}_{\text{N}}2$  Pre-Reaction Complexes? *Int. J. Mass Spectrom.* **2015**, *378*, 14–19.

- (23) Chen, J.; Xu, Y.; Wang, D. A Multilayered Representation, Quantum Mechanical and Molecular Mechanics Study of the  $\text{CH}_3\text{F} + \text{OH}^-$  Reaction in Water. *J. Comput. Chem.* **2014**, *35*, 445–450.

- (24) Yin, H.; Wang, D.; Valiev, M. Hybrid Quantum Mechanical/Molecular Mechanics Study of the  $\text{S}_{\text{N}}2$  Reaction of  $\text{CH}_3\text{Cl} + \text{OH}^-$  in Water. *J. Phys. Chem. A* **2011**, *115*, 12047–12052.

- (25) Xu, Y.; Wang, T.; Wang, D. A Multilayered-Representation Quantum Mechanical/Molecular Mechanics Study of the  $\text{S}_{\text{N}}2$  Reaction of  $\text{CH}_3\text{Br} + \text{OH}^-$  in Aqueous Solution. *J. Chem. Phys.* **2012**, *137*, 184501.

- (26) Möller, C.; Plesset, M. S. Note on an Approximation Treatment for Many-Electron Systems. *Phys. Rev.* **1934**, *46*, 618–622.

- (27) Adler, T. B.; Knizia, G.; Werner, H.-J. A Simple and Efficient CCSD(T)-F12 Approximation. *J. Chem. Phys.* **2007**, *127*, 221106.
- (28) Dunning, T. H., Jr. Gaussian Basis Sets for Use in Correlated Molecular Calculations. I. The Atoms Boron Through Neon and Hydrogen. *J. Chem. Phys.* **1989**, *90*, 1007–1023.
- (29) Raghavachari, K.; Trucks, G. W.; Pople, J. A.; Head-Gordon, M. A Fifth-Order Perturbation Comparison of Electron Correlation Theories. *Chem. Phys. Lett.* **1989**, *157*, 479–483.
- (30) Noga, J.; Bartlett, R. J. The Full CCSDT Model for Molecular Electronic Structure. *J. Chem. Phys.* **1987**, *86*, 7041–7050.
- (31) Kállay, M.; Gauss, J. Approximate Treatment of Higher Excitations in Coupled-Cluster Theory. *J. Chem. Phys.* **2005**, *123*, 214105.
- (32) Peterson, K. A.; Figgen, D.; Goll, E.; Stoll, H.; Dolg, M. Systematically Convergent Basis Sets with Relativistic Pseudopotentials. II. Small-Core Pseudopotentials and Correlation Consistent Basis Sets for the Post-*d* Group 16–18 Elements. *J. Chem. Phys.* **2003**, *119*, 11113–11123.
- (33) Werner, H.-J.; Knowles, P. J.; Knizia, G.; Manby, F. R.; Schütz, M.; et al. *Molpro*, version 2015.1, a package of ab initio programs, see <http://www.molpro.net>.
- (34) MRCC, a quantum chemical program suite written by Kállay, M.; Rolik, Z.; Ladjánszki, I.; Szegedy, L.; Ladóczki, B.; Csontos, J.; Kornis, B. See also: Rolik, Z.; Kállay, M. A General-Order Local Coupled-Cluster Method Based on the Cluster-in-Molecule Approach. *J. Chem. Phys.* **2011**, *135*, 104111. See also [www.mrcc.hu](http://www.mrcc.hu)
- (35) Szabó, I.; Czakó, G. Dynamics and Novel Mechanisms of  $S_N2$  Reactions on ab Initio Analytical Potential Energy Surfaces. *J. Phys. Chem. A* **2017**, *121*, 9005–9019.
- (36) Czakó, G.; Szabó, I.; Telekes, H. On the Choice of the ab Initio Level of Theory for Potential Energy Surface Developments. *J. Phys. Chem. A* **2014**, *118*, 646–654.
- (37) Ruscic, B.; Pinzon, R. E.; Morton, M. L.; von Laszewski, G.; Bittner, S.; Nijssure, S. G.; Amin, K. A.; Minkoff, M.; Wagner, A. F. Introduction to Active Thermochemical Tables: Several “Key” Enthalpies of Formation Revisited. *J. Phys. Chem. A* **2004**, *108*, 9979–9997.
- (38) Ruscic, B.; Bross, D. H. Active Thermochemical Tables (ATcT) Values Based on Ver. 1.122 of the Thermochemical Network (2016), available at [ATcT.anl.gov](http://ATcT.anl.gov).